

Low-Temperature Synthesis of Glass-Ceramics with $\text{YNbO}_4:\text{Tb}^{3+}$ Crystallites

© V.A. Kravets, E.V. Ivanova, M.A. Yagovkina, M.V. Zamoryanskaya

Ioffe Institute, St. Petersburg, Russia

e-mail: vladislav2033@yandex.ru

Received on April 15, 2021

Revised on April 15, 2021

Accepted on July 24, 2021

The main aim of this work was to perform low-temperature synthesis of glass-ceramics with $\text{YNbO}_4:\text{Tb}^{3+}$ crystalline inclusions and study the structural and luminescent properties of the samples synthesized. In the framework of this work, inclusions crystallized in the system $\text{B}_2\text{O}_5\text{--Na}_2\text{O--Y}_2\text{O}_3\text{--Nb}_2\text{O}_5\text{--Tb}_4\text{O}_7$ (Bura). It was shown that in this system, regardless of the precursors in the samples, $\text{YNbO}_4:\text{Tb}^{3+}$ in an amount of more than 70% of the total crystalline component. The most promising system for the synthesis of activated glass-ceramics with YNbO_4 proved to be synthesized from oxide precursors; it crystallized more than 95% $\text{YNbO}_4:\text{Tb}^{3+}$ of the total crystalline component. The luminescent properties of crystalline inclusions were studied using the local cathodoluminescence method. The composition and structure of glass ceramics were studied by methods X-ray spectral microanalysis and X-ray diffraction phase analysis.

Keywords: $\text{YNbO}_4:\text{Tb}^{3+}$, luminescence, glass-ceramics.

DOI: 10.21883/EOS.2022.14.53998.2083-21

Introduction

Yttrium niobate activated by rare earth ions (REI) is a promising radiation-resistant scintillator, in particular, an X-ray phosphor. Such materials can be used in medical and industrial radiography [1,2]. A promising direction is the development of methods for the synthesis of glass-ceramic materials activated with REIs. Such hybrid materials combine the properties of both glasses and crystals. Their synthesis and subsequent treatment are similar to the synthesis and treatment of glass, while the level of nonradiative losses during luminescence excitation are much lower than in glasses.

In the papers [3,4] the possibility of high-temperature synthesis of glass-ceramic materials with yttrium niobate crystallites was shown. In the course of previous studies [5,6] it was found that the boron-sodium oxide matrix is extremely promising for the low-temperature synthesis of REI-doped yttrium niobate.

Yttrium niobate has a high density, which is important when absorbing and converting ionizing radiation into visible light, is not hygroscopic, and also has high radiation and chemical resistance. Besides, yttrium niobate has its own wide luminescence band in the blue spectral range associated with NbO_4^{3-} complex [7]. Upon excitation by high-energy radiation of yttrium niobate, additionally activated by REI, the excitation is transferred from the levels responsible for the intrinsic luminescence of the matrix to the REI levels, which increases the luminescence yield of the activator upon absorption of ionizing radiation [8,9].

In the present paper studies on the low-temperature synthesis of yttrium niobate in a boron-sodium matrix are

continued. Tb^{3+} is used as an activator in this paper. Tb^{3+} ions in YNbO_4 crystals exhibit intense luminescence in the green range of the spectrum associated with energy transitions from 5D_4 levels [10,11].

The aim of this paper is to search for optimal precursors for the synthesis of glass ceramics with $\text{YNbO}_4:\text{Tb}^{3+}$ crystal inclusions. In this paper the inclusions crystallized in the system $\text{B}_2\text{O}_5\text{--Na}_2\text{O--Y}_2\text{O}_3\text{--Nb}_2\text{O}_5\text{--Tb}_4\text{O}_7$ (Bura) were studied. The study of the structure, composition, and optical properties of the synthesized materials was carried out by X-ray diffraction (XDPA), X-ray spectral microanalysis (XSMA), and local cathodoluminescence (CL) with a spatial resolution of $1\ \mu\text{m}$.

Samples synthesis

For the samples synthesis a sodium-boron matrix was used, since it proved to be the most promising for the synthesis of glass ceramics with YNbO_4 [5]. The sodium-boron matrix is characterized by a relatively low synthesis temperature under standard conditions (from 900°C). Yttrium, niobium, and terbium compounds were added to the matrix in such a proportion that the following molar ratios in terms of oxides were met in the synthesized material: $M(\text{Tb}_2\text{O}_3)/M(\text{Y}_2\text{O}_3) \leq 0.2$ and $M(\text{Tb}_2\text{O}_3 + \text{Y}_2\text{O}_3)/M(\text{Nb}_2\text{O}_5) \sim 1$.

The first ratio is determined by the optimal REI concentration in the yttrium niobate matrix, at which the maximum radiation intensity is observed [1]. The second ratio is chosen in such a way that, as a result of ceramic synthesis, crystal YNbO_4 is formed in it from melt [12]. To form crystallites in the material at the final stage of synthesis, the

Table 1. Sample composition Bura-Tb-1

Components	Weight, g	wt%	mol%
Tb ₄ O ₇	0.16	2.6	0.7
Y ₂ O ₃	0.47	7.6	7.1
Nb ₂ O ₅	0.675	10.9	8.7
Na ₂ B ₄ O ₇	4.9	79.0	83.4

Table 2. Sample composition Bura-Tb-2

Components	Weight, g	wt%	mol%
Tb ₄ O ₇	0.19	1.6	0.4
Y ₂ O ₃	0.565	4.7	4.4
NbCl ₅	1.65	13.7	10.7
Na ₂ B ₄ O ₇	9.65	80.0	84.4

samples were slowly cooled in a muffle furnace. Reagents with a purity of at least 99% were used as initial components for melting glasses.

a) Bura-Tb-1 sample

To synthesize the Bura-Tb-1 sample a multicomponent mixture was prepared: yttrium oxide, niobium oxide, terbium oxide, and sodium salt of boric acid were mixed in the ratios presented in Table 1 and placed in a ceramic crucible for further heat treatment at 900°C.

b) Bura-Tb-2 sample

To synthesize the Bura-Tb-2 sample a multicomponent mixture was prepared by dissolving terbium oxide, yttrium oxide, niobium chloride, and sodium salt of boric acid in nitric acid in the ratios shown in Table 2. Then the resulting composition was dried in an oven at 100°C until the liquid component was removed. The dried mass was heated for 15 min at 500°C, ground to a powder, and loaded into the ceramic crucible for subsequent melting at 900°C.

c) Bura-Tb-3 sample

For the synthesis of the Bura-Tb-3 sample, the mixture of initial components intended for further heat treatment was prepared as follows: terbium nitrate, yttrium nitrate, and niobium chloride were dissolved in isopropyl alcohol in the ratios indicated in Table 3.

Sodium tetraborate was added to the resulting mixture, thoroughly mixed, and dried in the oven at 100°C until the alcohol component was removed. As a result, a powder mass was obtained, which was loaded into the ceramic crucible for subsequent melting at 900°C.

The final stage of synthesis of all samples was carried out in the muffle furnace in the following mode: heating to 900°C — 1 h, holding at 900°C — 30 min and gradual cooling to room temperature during 3.5 h. Also note that for all samples a single charge material addition to the crucible was made during the final stage of synthesis, when the temperature inside the furnace reached 600°C.

Table 3. Sample composition Bura-Tb-3

Components	Weight, g	wt%	mol%
Tb(NO ₃) ₃ · 6H ₂ O	0.113	1.9	1.2
Y(NO ₃) ₃ · 6H ₂ O	0.47	7.9	6.1
NbCl ₅	0.41	6.9	5.4

Research methods

The homogeneity of the samples and the presence of inclusions were studied in an optical microscope of the CL-system. The elemental composition of the samples was determined using the XSMA method. The luminescent properties were studied by the CL method. The presence of crystal inclusions in the samples was determined by the XDPA method. The distribution of crystal conglomerates in the sample was studied in CL-microscope.

XDPA-studies were carried out using D2 Phaser X-ray diffractometer (Bruker, Germany). To identify the crystal component in the samples the Inorganic Crystal Structure Database (ICSD) data were used: YNbO₄ Fergusonite — beta (Y) 00-023-1486, NaCl Halite 01-080-3939, NaNbO₃ Sodium niobite (V) 01-077-0261, Y₂O₃ 01-076-0151 and YBO₃ Yttrium borate 01-074-1929.

To study the samples by CL and XSMA methods, we used CAMEBAX electron probe microanalyzer (Cameca, France) combined with CL-station of an original design [13]. The equipment used makes it possible to obtain spectra with a lateral resolution from 1 μm, which makes it possible to study the homogeneity of the luminescent properties of samples and CL-images, which can be used to evaluate the homogeneity of CL-sample and inclusion sizes from ~ 1 μm. The CL spectra were obtained at an electron accelerating voltage of 20 kV, an absorbed current of 10 nA, and an electron beam diameter of 3 μm. At such accelerating voltage, the CR generation region has a depth of about 3 μm. CL-images were obtained with an electron beam diameter of 200 μm, electron accelerating voltage of 20 kV, and absorbed current of 20 nA.

The locality of the ESMA method, as well as of the CL method, can vary in the range of 1 to 200 μm. The composition of the samples was measured at electron accelerating voltage of 20 kV, absorbed current of 15 nA, and electron beam diameter of 3 μm. To measure Y, Nb and Tb the compounds of Nb, Y₃Al₅O₁₂ and TbPO₄ were used as standards. The oxygen content was calculated based on stoichiometry. Due to the fact that it was not possible to measure Na, the content of elements was calculated on the assumption that the matrix consisted of boron oxide. This approximation was made based on the fact that the absorption of Na- and B-characteristic lines of the measured elements differs slightly. For each sample, at least five analyzes of the matrix composition in random areas were performed. This made it possible to obtain an average

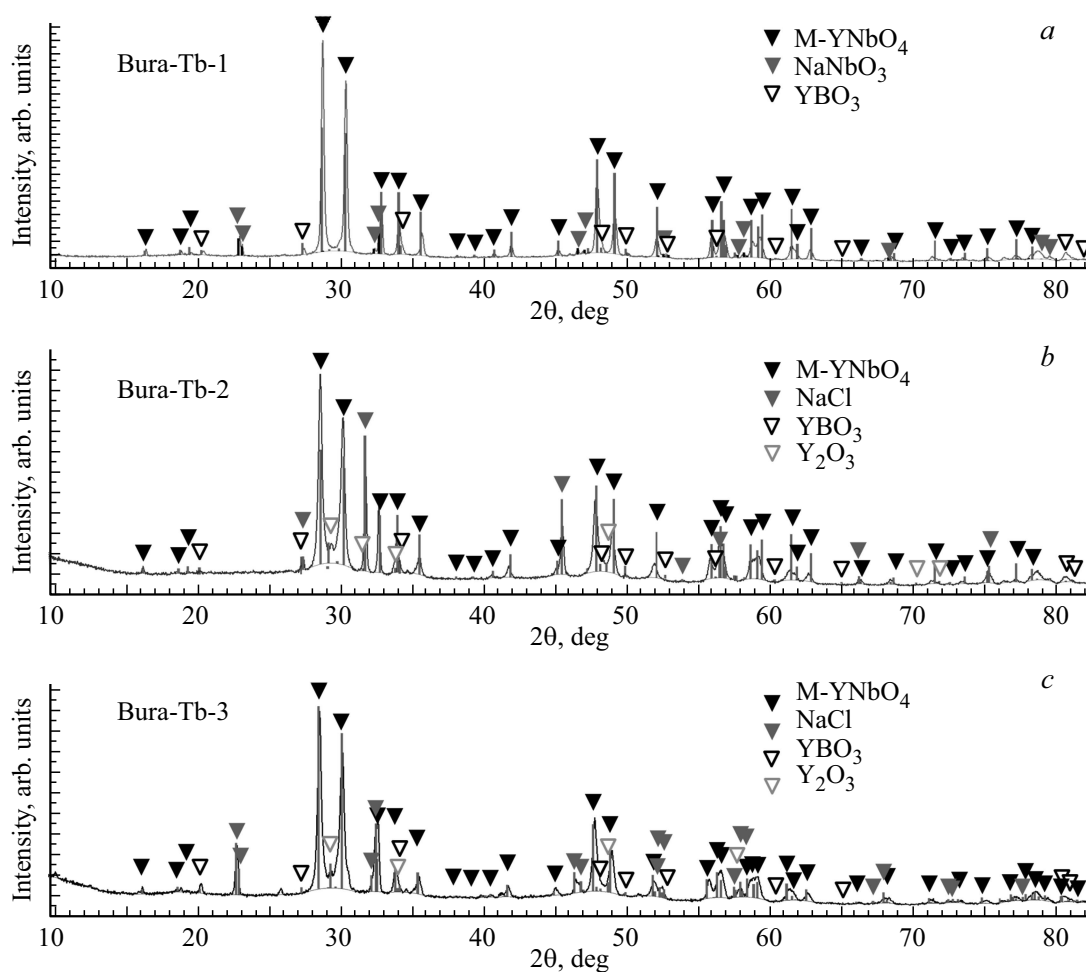


Figure 1. Diffraction curves of samples Bura-Tb-1 (a), Bura-Tb-2 (b), Bura-Tb-3 (c).

elemental composition and to evaluate the uniformity of the elements distribution in the samples.

CL- and ESMA- studies are carried out on the same device, which makes it possible to analyze the composition and to record CL spectra in the same region of the sample. This simplifies the interpretation of the contrast of CL-images.

Results and discussions

XDPA

XDPA results for the synthesized samples are shown in Fig. 1 and Table 4. It is shown that each of the samples contains various crystal inclusions. The detected crystal phases and their content in relative percentages of the total crystal phase in the sample are given in Table 4.

Also, the diffraction curves for all Bura-Tb samples show wide „halos“ in the range 15° – 22° , 25° – 38° and 40° – 55° angles 2θ , characteristic of the X-ray amorphous component of the sample (Fig. 1, a, b, c).

The peaks on the diffraction curves for all samples were interpreted. It was determined that YNbO_4 crystallized in

all samples, however, other compounds (NaNbO_3 , YBO_3 , NaCl , Y_2O_3) additionally crystallized. This suggests that further optimization of the synthesis conditions is necessary. NaCl crystallization in the Bura-Tb-2 sample indicates insufficient synthesis temperature. More than 95% of the crystal M-YNbO_4 -phase was formed in the Bura-Tb-1 sample, this is significantly more than in Bura-Tb-2 and Bura-Tb-3 images.

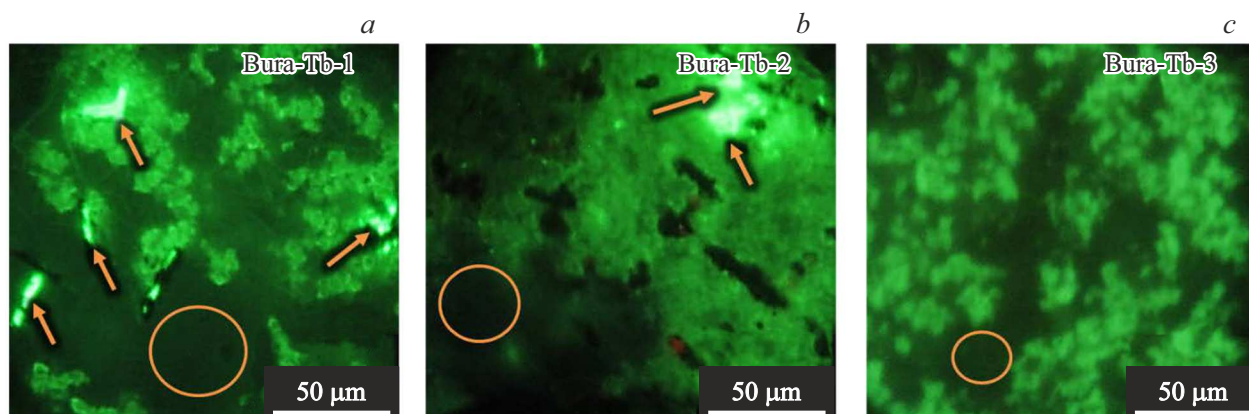
CL-microscopy and RSMA-studies

Figure 2 shows CL-images of the samples. On the CL-images of all the samples, uniform regions are observed (marked by a circle in Fig. 2). Also, the CL-images of all samples (Fig. 2) exhibit a color contrast typical for micron and submicron crystal inclusions doped with Tb^{3+} . The fraction of inclusions observed on the CL-image of the samples surface, and their composition measured by the ESMA method, are presented in Table 4.

CL-images of Bura-Tb-1 sample (Fig. 2, a) demonstrate two types of inclusions. The first type (I) of inclusions has a much more intensive CL (marked in Fig. 2, a by an arrow). Such inclusions are extremely rare (less than 1% of the studied area of the sample). According to

Table 4. Characteristics of identified crystal inclusions

Sample	XDPA analysis of the crystal sample phases		CL-microscopy	XSMA
	Crystal phase	Relative percentage of total crystal phase in sample	Fraction of inclusions on surface of sample, %	Composition of identified crystallites
Bura-Tb-1	M-YNbO ₄	≥ 95	≥ 50	(Y _{0.77} Tb _{0.23})NbO ₄
	NaNbO ₃	≤ 3	–	–
	YBO ₃	≤ 2	~ 1	(Y _{0.83} Tb _{0.17})BO ₃
Bura-Tb-2	M-YNbO ₄	~ 70	≥ 50	(Y _{0.79} Tb _{0.21})NbO ₄
	NaCl	~ 25	–	–
	YBO ₃	≤ 3	~ 1	(Y _{0.82} Tb _{0.18})BO ₃
	Y ₂ O ₃	≤ 3	–	–
Bura-Tb-3	M-YNbO ₄	~ 70	≥ 50	(Y _{0.77} Tb _{0.23})NbO ₄
	NaNbO ₃	~ 25	–	–
	Y ₂ O ₃	≤ 3	–	–
	YBO ₃	≤ 2	–	–

**Figure 2.** CL-images of samples (a) Bura-Tb-1, (b) Bura-Tb-2 and (c) Bura-Tb-3.

XDPA data Nb was absent in these inclusions, Y and Tb were registered in significant amounts, the average concentration of Tb was 17 ± 1 at% by Y. The second type (II) of inclusions represents conglomerates with lateral size from 10 to $100 \mu\text{m}$, unevenly distributed over the sample and covering about 50% of the observed area of the sample. According to XSMA data the inclusions have the composition (Y,Tb)NbO₄ with a concentration of Tb 23 ± 1 at% by Y. In the region without visible inclusions (marked with a circle in Fig. 2) the content of Nb, Y, and Tb was measured. Their content was 0.7 ± 0.2 , 3 ± 0.5 and 0.5 ± 0.2 wt% respectively. The data are shown in Table 4.

In the Bura-Tb-2 sample, as well as in the Bura-Tb-1 sample, two types of inclusions were observed. These

inclusions are similar in their luminescent properties to the inclusions found in Bura-Tb-1. The first type (I) of inclusions (marked in Fig. 2, b by an arrow) occupies less than 1% of the sample area under study. According to XSMA data these inclusions contained no Nb, and the average concentration of Tb was 18 ± 1 at% by Y. The second type (II) of inclusions represents regions (with lateral size of more than $400 \mu\text{m}$), which are observed on more than 50% of the sample surface. In these areas, the crystallites are visually distributed uniformly, considering the locality of the method, in several μm . According to the ESMA data, these inclusions have the composition (Y,Tb)NbO₄ with concentration of Tb 21 ± 1 at% by Y. In the region without inclusions (marked with a circle in

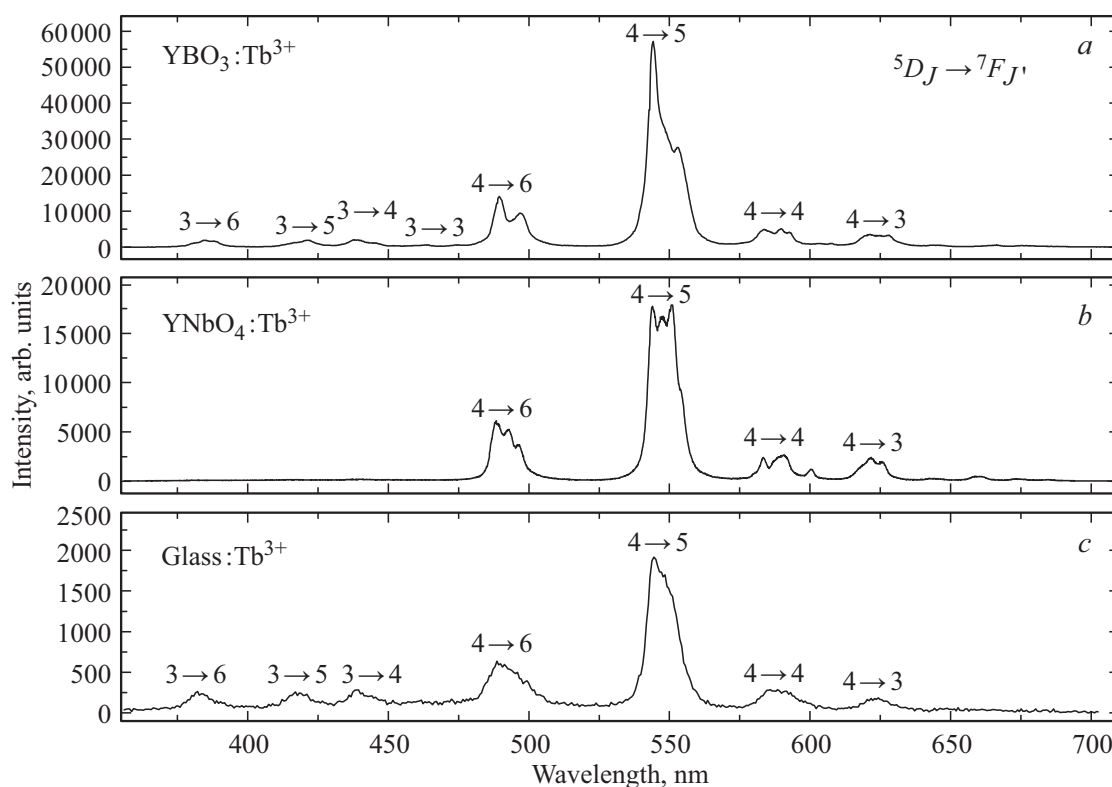


Figure 3. CL-spectra on a linear scale, characteristic for inclusions (a) of the first type (I), (b) of the second type (II), (c) from regions without inclusions. In CL-spectra above the bands associated with energy transitions Tb^{3+} , the corresponding quantum numbers $J \rightarrow J'$ are specified.

Fig. 2, b), the content of Nb was 4 ± 1 wt%, the content of Y and Tb is extremely low and is not registered by the device.

In the Bura-Tb-3 sample, only the second type (II) of inclusions was observed (Fig. 2, c). Inclusions are unevenly distributed over a significant part of the sample area under study. According to the XSDPA data, these inclusions have the composition $(\text{Y,Tb})\text{NbO}_4$ with concentration of Tb 23 ± 1 at% by Y. In the region without inclusions the content of Nb was 3 ± 1 wt%, the content of Y and Tb is extremely low and is not registered by the device.

CL spectra

Figure 3, a, b, c shows the CL spectra characteristic for certain regions of all samples. Also, for a more detailed analysis, the spectra are presented on semilogarithmic scale (Fig. 4, a, b, c). The spectra were interpreted in accordance with the paper [14].

The CL spectra of the first type (I) inclusions are shown in Figs 3, a and 4, a (these inclusions are found in samples Bura-Tb-1 and Bura-Tb-2 and are marked with arrows in Fig. 2).

Summing up the XSDPA, XSDMA, and CL data, we can confidently say that the first type (I) inclusions found in the samples Bura-Tb-1 and Bura-Tb-2 are crystal inclusions

$\text{YbO}_3:\text{Tb}^{3+}$. The shown CL-spectra of these inclusions (Figs. 3, a and 4, a) show bands associated with energy transitions Tb^{3+} from levels ${}^5D_3-{}^7F_J$ ($J = 6, 5, 4, 3, 2$) and ${}^5D_4-{}^7F_J$ ($J = 6, 5, 4, 3, 2, 1, 0$). The shape of the spectrum corresponds to the spectrum of Tb^{3+} in YbO_3 [15], where REIs replace Y ions with a local position S_6 [16,17].

The luminescence spectra in Figs. 3, b and 4, b correspond to the second type (II) inclusions. These inclusions are found in all samples. Also, summarizing the XSDPA, XSDMA, and CL data, we can conclude that second type (II) inclusions are $\text{YNbO}_4:\text{Tb}^{3+}$ crystallites. In the shown CL-spectra of these inclusions (Figs. 3, b and 4, b) there are bands associated with energy transitions Tb^{3+} from levels ${}^5D_3-{}^7F_J$ ($J = 6, 5, 4$) and ${}^5D_4-{}^7F_J$ ($J = 6, 5, 4, 3, 2, 1, 0$), while transitions from 5D_3 levels have an extremely low CL intensity and are noticeable only on semilogarithmic scale. The shape of the spectrum corresponds to the spectrum of Tb^{3+} in YNbO_4 [10,11], where REIs replace Y ions with a local position C_2 [5].

The CL-spectra shown in Figs. 3, c and 4, c were obtained in regions without inclusions (marked by circles in Fig. 2). In these spectra the bands associated with energy transitions Tb^{3+} from levels ${}^5D_3-{}^7F_J$ ($J = 6, 5, 4$) and ${}^5D_4-{}^7F_J$ ($J = 6, 5, 4, 3$) are observed. The shape of the spectrum corresponds to the spectrum of Tb^{3+} in borate glasses [18], where REIs occupy local positions close to C_{2v} [16].

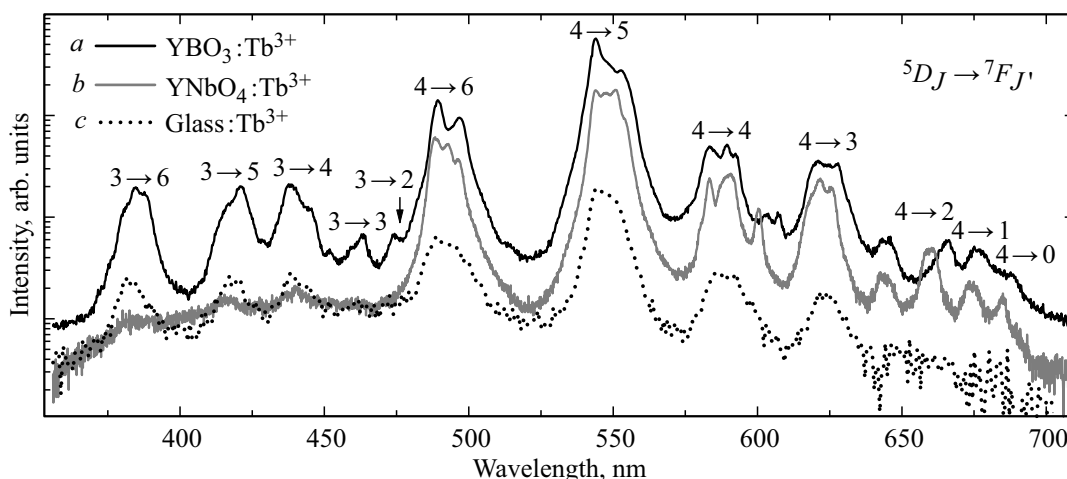


Figure 4. CL-spectra on semilogarithmic scale, characteristic for inclusions (a) of the first type (I), (b) of the second type (II), (c) from regions without inclusions. In CL-spectra above the bands associated with energy transitions Tb^{3+} , the corresponding quantum numbers $J \rightarrow J'$ are specified.

The obtained spectra correspond to the terbium radiation in materials with different local symmetry (Figs. 3 and 4). It was possible to confirm by the CL method that inclusions of yttrium niobate activated with Tb^{3+} , i.e. the second type (II) inclusions, crystallized in all samples. We also managed to confirm the presence of yttrium borate inclusions activated by Tb^{3+} (first type (I) inclusions) in Bura-Tb-1 and Bura-Tb-2 samples.

Conclusion

The low-temperature glassceramics with $YNbO_4$ doped with Tb, based on a promising sodium-borate matrix from various precursors have been synthesized for the first time. It can be seen from the presented results that NaCl, $NaNbO_3$, Y_2O_3 , and YBO_3 crystallites can additionally form in the samples during synthesis from various precursors. In all samples, the content of M- $YNbO_4$ is 70% minimum of the total crystal phase in the sample. It is also shown that the highest relative percentage of M- $YNbO_4$ is obtained during synthesis from oxide components, which makes this method of synthesis the most promising. It is shown that Tb enters into $YNbO_4$ crystallites in the amount of 21–23 at% by Y.

Acknowledgments

XDPA-studies were performed using the equipment of the Federal Common Research Center „Materials Science and Diagnostics in Advanced Technologies“, supported by the Ministry of Education and Science of Russia (unique project identifier: RFMEFI62119X0021). The authors are grateful to M.I. Moskvichev and V.V. Vaskevich for the samples provided.

Conflict of interest

The authors declare that they have no conflict of interest.

References

- [1] Mester A.Yu., Mester A.Yu., Mozharov A.M., Trofimov A.N., Zamoryanskaya M.V. // Opt. and spectr. 2016. V. 120. № 5. P. 768–774 (in Russian).
- [2] Nazarov M., Kim Y.J., Lee E.Y., Min K.I., Jeong M.S., Lee S.W., Noh D.Y. // J. Appl. Phys. 2010. V. 107. N 10. P. 103104.
- [3] Dymshits O.S., Alekseeva I.P., Zhilin A.A., Tsenter M.Y., Loiko P.A., Skoptsov N.A., Malyarevich A.M., Yumashev K.V., Mateos X., Baranov A.V. // J. Lumin. 2015. V. 160. P. 337–345.
- [4] Loiko P.A., Dymshits O.S., Alekseeva I.P., Zhilin A.A., Tsenter M.Y., Vilejshikova E.V., Yumashev K.V. // J. Lumin. 2016. V. 179. P. 64–73
- [5] Kravets V.A., Ivanova E.V., Orekhova K.N., Gusev G.A., Vaskevich V.V., Moskvichev M.I., Zamoryanskaya M.V. // Opt. and spectr. 2021. V. 29. № 2. P. 207–213 (in Russian).
- [6] Kravets V.A., Ivanova E.V., Zamoryanskaya M.V. // J. Phys.: Conference Series. 2020. V. 1697. N 1. P. 012163.
- [7] Dačanin L.R., Lukić-Petrović S.R., Petrović D.M., Nikolić M.G. // J. Lumin. 2014. V. 151. P. 82–87.
- [8] Blasse G., Bril A. // J. Electrochem. Soc. 1968. V. 115. P. 1067–1075.
- [9] Blasse G., Bril A. // J. Lumin. 1970. V. 3. P. 109–131.
- [10] Liu X., Lü Y., Chen C., Luo S., Zeng Y., Zhang X., Lin J. // J. Phys. Chem. C. 2014. V. 118. P. 27516–27524.
- [11] Boutinaud P., Cavalli E., Bettinelli M. // J. Phys.: Condensed Matter. 2007. V. 19. N 38. P. 386230.
- [12] Galakhov F.Ya. Diagrammy sostoyanij sistem tugoplavkikh oksidov. Spravochnik. Vyp. 5. P. 2. Nauka, 1986 (in Russian).
- [13] Zamoryanskaya M.V., Konnikov S.G., Zamoryanskii A.N. // Instrum. Exp. Tech. 2004. V. 47. P. 477–483.

- [14] *Leavitt R.P., Gruber J.B., Chang N.C., Morrison C.A.* // J. Chem. Phys. 1982. V. 76. P. 4775–4788.
- [15] *Sato R., Takeshita S., Isobe T., Sawayama T., Niikura S.* // ECS J. Solid State Sci. Technol. 2012. V. 1. N 6. P. R163.
- [16] *Kravets V.A., Ivanova E.V., Orekhova K.N., Petrova M.A., Gusev G.A., Trofimov A.N., Zamoryanskaya M.V.* // J. Lumin. 2020. V. 226. P. 117419.
- [17] *Yin X., Zhao Q., Shao B., Lv W., Li Y., You H.* // Cryst. Eng. Commun. 2014. V. 16. P. 5543.
- [18] *Wada N., Kojima K.* // Opt. Mat. 2013. V. 35. N 11. P. 1908–1913.